New radar Micro-Doppler tag for road safety based on the signature of rotating backscatters

A. Lazaro, *Senior Member, IEEE*, M. Lazaro, R. Villarino and P. de Paco, *Senior Member, IEEE*

***Abstract*—This work asses a way to improve the detection of pedestrians, workers or cyclists, but also other static elements on the road. These elements due to its low radar cross-section can be masked by other larger objects close to them, when they are illuminated by an automotive radar. Rotating backscatter is proposed to enhance the detection with automotive FMCW radars due to the introduction of a differentiable micro-Doppler signature. A comprehensive theory of operation is explained in this paper. Simulated and experimental results are presented at 24 GHz for transponder detection in presence of strong clutter in range-velocity maps.**

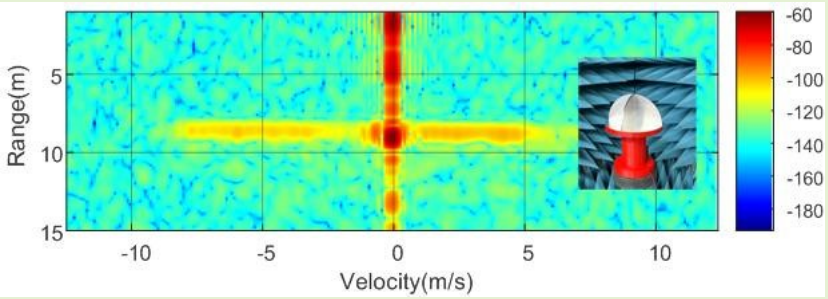

***Index Terms*— Backscattering, FMCW radar, Micro-Doppler, Modulated transponder, pedestrian detection, millimeter band sensors, RFID.**

I. Introduction

AUTOMOTIVE radar is expected to be a fast-growing market to improve safety and comfort. These radars carry out a crucial role in helping drivers, maintaining safe distances, and avoiding collisions. A radar is a key sensor for advanced driver assistance systems (ADAS) for future generations of autonomous vehicles [1]. Pedestrians or cyclists collisions with vehicles on the roads are unfortunately frequent under low illumination conditions at night or bad weather conditions [2][3]. Radar sensors are a complement to computer vision techniques, with the advantage that radars are less affected under these environmental conditions [4]. In recent years, there has been significant progress in mmWave technology and the expensive GaAs-based technology is being replaced by the less expensive SiGe technology [5]. The 24 GHz band is temporally allocated for short-range radars (SRR). The 77 GHz band is allocated for long-range radars (LRR). Figure 1 compares the range of measured RCS of different objects of interest (vehicles, pedestrians, and guardrails) [6]. The RCS behavior of these objects is complex and depends on the orientation and the vehicle model and size. The average RCS of a pedestrian at 24 GHz is about -5 dBsm [7]. This value is significantly lower than a typical car (10 dBsm), a motorcycle (5-8 dBsm) [8] or a guardrail (5-10 dBsm) [9]. The values at 77 GHz band are typically about 5-7 dB higher than at 24-26 GHz band. Besides, the speed of pedestrians and bikes is very low (<15 km/h for pedestrians), therefore pedestrians can be confused with clutter due to large static objects such as ground or metallic objects (such as traffic signals, guardrails, etc) [10]. Besides, ground and big reflectors such as guardrails introduce multipath reflections that make it difficult to detect these sensible road objects. A post-processing technique has recently been introduced in [11] to mitigate multipath. This situation is common with bikes circulating on the verge of roads or workers repairing roads.

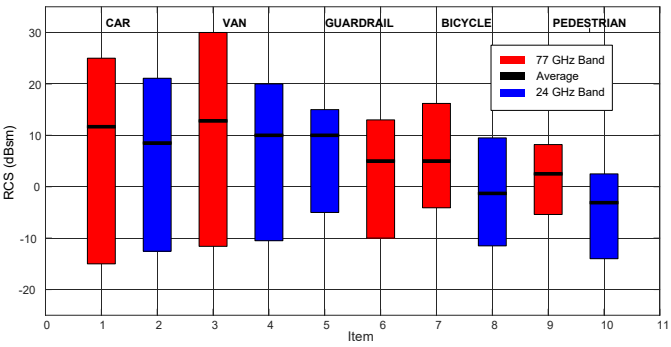

Fig. 1. Comparison of RCS from different relevant objects: car, small van, guardrail, bicycle, and pedestrian [6][9].

The novelty of this work is to study the feasibility of using modulated backscattering tags inducing a phantom Doppler signature to improve the detection in front of static clutter interference. The tag is based on a rotating corner reflector that introduces a micro-Doppler signature providing additional information for target recognition. Rotating parts, such as

Manuscript received October 12, 2020. This work was supported by the Spanish Government Project RTI2018-096019-B-C31 and grant PRE2019-089028.

A. Lazaro, M. Lazaro, R. Villarino are with the Electronics, Electrical and Automatics Engineering Department, Universitat Rovira i Virgili, 43007 Tarragona, Spain (antonioramon.lazaro@urv.cat, phone: +34-977.55.86.68).

P.de Paco is with Telecommunications and Systems Engineering Department, Universitat Autonoma de Barcelona (UAB), Spain.

blades or rotating antennas, introduce periodic modulation in the turn back signals when are illuminated by the radar [12][13][14][15]. The micro-Doppler introduced by the rotor of small Unmanned Aerial Vehicles (UAVs) has been proposed to enhance the discrimination between the UAV and the clutter and detect their presence at long distances [16][17]. Several time-frequency analysis techniques have been proposed to extract features and detecting target for this application [18][19]. The technique most extended is the Short-time Fourier Transform (STFT) obtained from the computation of Fourier transform in a long-time window. Advanced techniques have been recently proposed for identification based on the measurement of the Helicopter Rotation Modulation (HERM) lines that are a function of the blades rotation rate and the number of blades [20]. The utilization of mm-wave FMCW radar for this application has arisen in the last years [21].

Indeed, this modulation can be used for tag identification [22]. This approach is easily implementable even at millimeter-wave bands where high radar cross-section can be obtained with the use of corner reflectors [23][24]. These tags can be located as warning signals on the road, to indicate the presence of workers moving near the vehicles on the road. The tag could be also mounted on cycles to improve their detection. The movement of a pedestrian is very complex and therefore it is difficult to identify by the radar and distinguish from other clutter sources, whereas the proposed tag has a strong echo with a particular signature in Doppler domain that, as will be studied, makes it easier to detect. Range-Doppler map is a frequently used tool in automotive FMCW radars to shows the velocity and range of the detected targets. In this work, the Doppler beamwidth in the range-Doppler map more than the HERM lines is the feature that is used to identify the tag. Therefore, the proposed detection method does not require additional hardware in the vehicle because the FMCW radar is also used as a reader.

The paper is organized as follows. Section II deals with the basic theory of detection of the micro-Doppler signature by FMCW radar from the range-Doppler matrix. Section III and Section IV present simulated and experimental results, respectively. Finally, Section V draws the conclusions.

II. Range-Doppler Signature and System Operation

A model for the proposed system is shown in Fig. 2. Let us begin with a simple case, where a backscatter (P) rotates around a center point (O) in the horizontal plane with an angular rotation rate (Ω). Ω can be controlled by the spinning motor speed. It is assumed that both radar and the transponder are in the same plane, therefore the elevation angle is close to zero. D demotes the distance from the backscatter point P to the rotation center (O), and R_0 is the distance between the radar and the center.

Considering that $D<<R_0$, the range from the radar to the backscatter point can be approximated by:

$$r(t) \approx R_0 + v \cdot t + Dsin(\theta_0 + \Omega t) = R_0 + v \cdot t + Dsin(\theta_0)cos(\Omega t) + Dcos(\theta_0)sin(\Omega t), \quad (1)$$

where θ_0 is the initial angle at t=0 and v is the relative radial velocity of the target with respect to the radar.

The phase shift due to the propagation is

$$\phi(t) = -2kr(t) = -\frac{4\pi}{\lambda_c} r(t) \quad (2)$$

Where k is the wavenumber and λ_c is the central wavelength at which the radar illuminates the target. The Doppler frequency shift (f_D) of the received signal from the backscatter can be obtained using

$$f_D = \frac{1}{2\pi}\frac{d\phi(t)}{dt} = -\frac{2v}{\lambda_c} - \frac{2D\Omega}{\lambda_c}\cos(\Omega t + \theta_0) \quad (3)$$

The first term in (3) is the frequency Doppler shift due to the linear movement between the radar and the target, whereas the second term is the periodical micro-Doppler shift introduced by the rotation of backscatter point (P). Notice that if the distance D or the rotation rate Ω are small, then the conventional expression of the Doppler shift is recovered. As expected the larger D, the larger radar cross-section (RCS) of the tag.

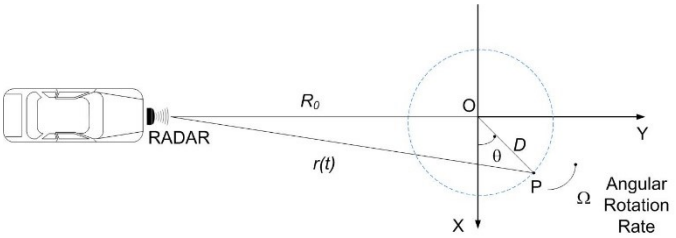

Fig. 2. System geometry composed by an automotive radar and a tag based on a rotating reflector.

Automotive radars are based on frequency-modulated continuous-wave radar (FMCW) due to the ability of these radars to measure simultaneously the target range and its relative velocity. To this end, the transmission frequency is swept as shown in Fig. 3 in which a block diagram of a typical FMCW radar is shown. The complex transmitted FMCW signal $x_T(t)$ is composed of chirps and can be expressed as:

$$x_T(t) = \sum_{l=0}^{\infty} x_c(t - lT), \quad (4)$$

with $x_c(t)$ is a chirp signal of duration T:

$$x_c(t) = Ae^{j2\pi\left(f_c t + \frac{1}{2}\mu t^2\right)} \prod\left(\frac{t}{T}\right) \quad (5)$$

Where $\prod(t)$ denotes a rectangular pulse signal, A is the amplitude, f_c is the carrier frequency and $\mu=B/T$ is the sweeping slope, T is the sweep period and $B=f_{max}-f_{min}$ is the bandwidth. The backscattered received signal $x_R(t)$ is the transmitted signal delayed by the propagation delay $\tau=2r(t)/c$ and its amplitude is proportional to the radar cross-section of the rotation target, $\sigma(t)$:

$$x_R(t) = A'\sqrt{\sigma(t)}x_c(t - \tau) \quad (6)$$

Where A' takes into account the attenuation due to the propagation. The beat signal is obtained low-pass filtering the signal at the Intermediate Frequency (IF) that comes from the output of the mixer:

$$x_{IF}(t) = x_R(t) \cdot x_c^*(t) = \sum_{l=0}^{\infty} y(t - lT) \quad (7)$$

$$y(t) = A''\sqrt{\sigma(t)} \prod\left(\frac{t}{T}\right) \cdot e^{-j2\pi\left(f_c\tau - \frac{\mu\tau^2}{2}\right)} e^{-j2\pi\mu\tau t} \quad (8)$$

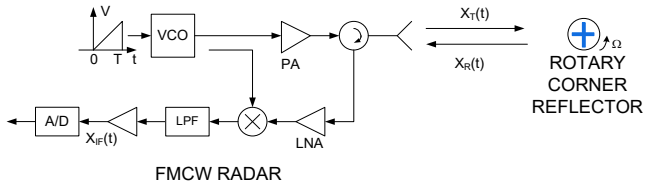

Fig. 3. Block diagram of a typical FMCW radar illuminating a rotary corner reflector.

By approximating the delay from that happened at the beginning of each ramp, $\tau \approx \tau_0+2v/c(lT)+(2D/c)\sin(\Omega t+\theta_0)$, and neglecting quadratic terms, which are valid if μ and v are reasonably small, then the IF-output signal is:

$$y(t) \approx A''\sqrt{\sigma(t)}\prod\left(\frac{t}{T}\right)\cdot e^{-j2\pi\left(f_c\tau_0-\frac{\mu\tau_0^2}{2}\right)}e^{-j2\pi\mu\tau_0 t}e^{j2\pi f_{D0}lT}e^{-j\beta\sin(\Omega t+\theta_0)} \quad (9)$$

Where A'' is the amplitude at the IF-output due to the conversion gain of the mixer and $f_{D0}=-2vf_c/c$ is the Doppler frequency shift due to linear movement. β is the non-dimensional parameter known in FM signals as modulation index $\beta=4\pi D/\lambda_c$, being λ_c the wavelength at the central frequency ($\lambda_c=c/f_c$). Let's check the output signal shown in (9), the first factor in (9) represents an amplitude term, the second is due to the time-of-arrival (TOA), the third product is related to the Doppler shift and the fourth factor is the periodic modulation effect due to the backscatter rotation. The period of this last term is equal to the revolution period $T_r=2\pi/\Omega$ and therefore it can be expanded in series of Fourier:

$$e^{-j\beta\sin(\Omega t+\theta_0)} = \sum_{n=-\infty}^{n=+\infty} c_n e^{jn\Omega t} = \sum_{n=-\infty}^{n=+\infty}(-1)^n e^{jn\theta_0}J_n(\beta)e^{jn\Omega t} \quad (10)$$

Where $J_n(x)$ is the Bessel function of first kind defined by:

$$J_n(x) = \frac{1}{2\pi}\int_{-\pi}^{\pi} e^{j(x\sin(u)-nu)}du \quad (11)$$

In the fast-ramp-based FMCW radar, the received IF signal is digitalized by the ADC with sampling frequency f_s and the samples are stored into a matrix $s(k,l)$, k=0…N-1, l=0…L-1.

$$s(k,l) = A''\sum_{l=0}^{\infty}\prod\left(\frac{kT_s}{T}\right)\sqrt{\sigma(lT)}\cdot \sum_{n=-\infty}^{+\infty} c_n e^{-j2\pi(f_c\tau_0-\frac{\mu\tau_0^2}{2})}e^{-j2\pi\mu\tau_0 kT_s}e^{j2\pi f_{D0}lT}e^{jn\Omega(kT_s+lT)} \quad (12)$$

FMCW radars are used in automotive radar to detect the range and velocity of the targets through the range-velocity map [25](see Fig.4). The range-velocity map, also known as range-Doppler map (RD), is obtained from two-dimensional FFT of a frame $s(k,l)$ which is composed of L chirps with N samples by chirp [26]. First, an FFT (range FFT) is applied to each chirp signal giving the range position of the echoes. This procedure is repeated for each of the L chirp signals of the frame. The result of each FFT in range is stored in a column of a two-dimensional matrix. The Doppler frequency (or velocity) is obtained for each range gate by applying a second FFT (Doppler FFT) inside each range gate. Therefore, the FFT is applied to each row of the two-dimensional matrix. The result is stored in the range-Doppler-matrix (RDM). In order to reduce the side-lobe interference a windowing is used. Zero padding method is used to improve the accuracy. The procedure of computation of the RDM is shown in Figure 4.

From (12), the response of the tag in the RDM will be a set of peaks located at $k=\mu\tau_0-n\Omega\approx\mu\tau_0$, which correspond to the range position of the tag (assuming that shift introduced by the rotation is negligible) and at $l=f_{D0}+n\Omega/2\pi$, Doppler shift due to movement relative to the radar and Doppler associated to the rotation respectively. The amplitudes of these peaks are modulated by the Fourier coefficient c_n. However, as it will be shown later, sometimes these peaks are below the Doppler (velocity) resolution due to windowing effects in the FFTs.

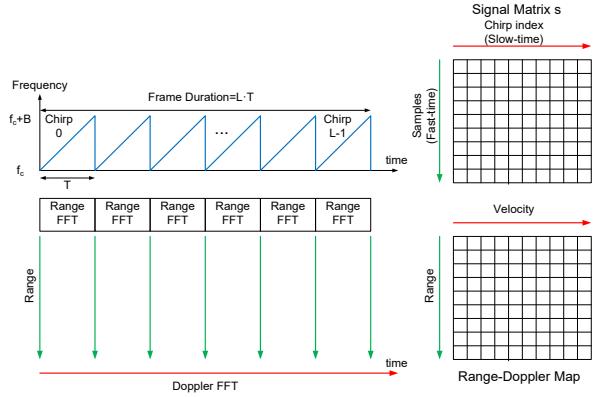

Fig. 4. Signal sampling and range-Doppler matrix calculation from 2D Fourier Transforms.

III. SIMULATED RESULTS

Fig.5 shows the amplitude of the Fourier coefficients (C_n) of the Doppler induced by the rotation for different values of the modulation index β. The bandwidth can be approximated as in the case of a frequency modulated (FM) signal by the Carson rule: BW$\approx 2(\beta+1)f_r$, where $f_r=\Omega/2\pi$ is the rotation frequency. The bandwidth matches up to the maximum Doppler frequency shift ($2D\cdot\Omega/\lambda_c$) for high values of β.

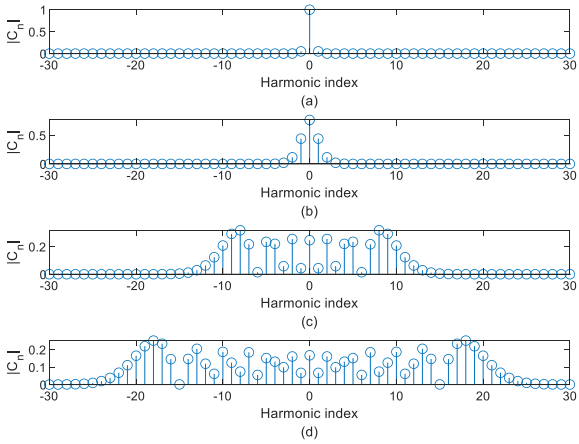

Fig. 5. Amplitude of the Fourier coefficients C_n as a function of the harmonic index for different values of modulation index β: (a) β =0.1, (b) β =1, (c) β =10, (d) β =20.

For an N-blade rotor, there are N scatters at different initial rotation angle [12]:

$$\theta_k = \theta_0 + k\frac{2\pi}{N}, k = 0,1 \dots N-1 \qquad (13)$$

The result is the superposition of the backscatter echoes. Fig.6. shows the amplitude of the Fourier coefficients for a 4-blade rotor. It is assumed that the radar cross-section of each backscatter is the same. Considering the constructive and destructive contributions, the equivalent scenario is a system that rotates four (N) times faster, being the amplitude four (N) times higher (N=4). On the other hand, neither the bandwidth, which depends on the modulation index nor the rotation frequency, change with respect to the case with only one backscatter.

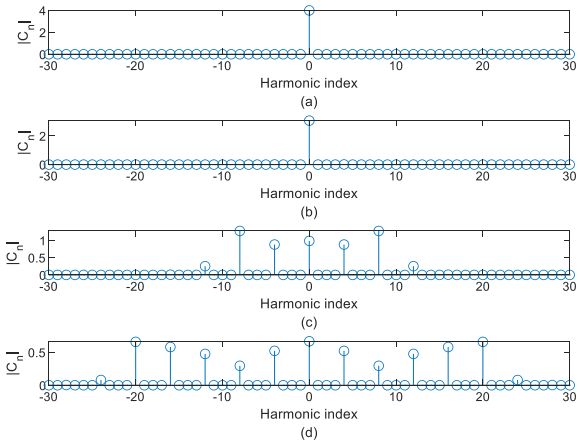

Fig. 6. Amplitude of the Fourier coefficients C_n for a 4-blade rotor as a function of the harmonic index for different values of modulation index β: (a) β =0.1, (b) β =1, (c) β =10, (d) β =20.

In order to show pieces of evidence of the feasibility to detect the proposed transponder in complex scenarios, several simulations have been performed. The scenario is composed of a car with a radar on board and another car driving on the same lane at a speed of 8 m/s faster than the radar and a RCS of 18 dBsm. A stationary rotating corner is located at the right side and it presents a radar cross-section of -10 dBsm (for example to emulate the RCS of a worker, pedestrian or cyclist). The worst-case for detection has also been considered, which is one in which the speed is similar to that of larger objects around or it moves at a very slow speed. Behind the transponder, there are three trees with an RCS of 10 dBsm (see Fig.7).

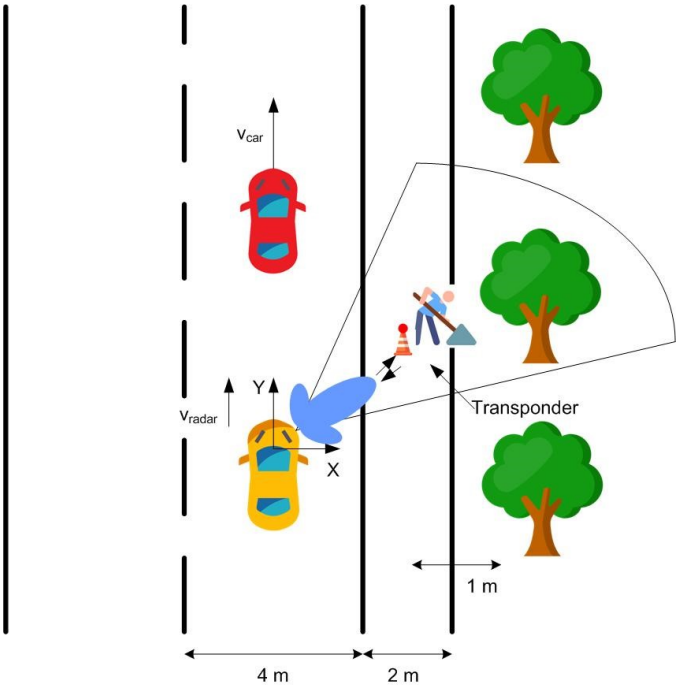

Fig. 7. The scenario used in the simulations

When the radar is in motion, the fixed targets like the corner and the trees have a relative velocity of – 5 m/s (assuming that the vehicle with the radar is moving at 5 m/s). The simulations have been performed with a FMCW radar with the same parameters than the radar used for the experimental verification (see Table I). The radar sweeps from 24-24.3 GHz with a sweep time of 256 μs and a sampling frequency of 1.2 MHz. The number of points per chirp N was 256 and the number of frames L=128. The Hann window (Hanning window) was considered. Fig.8a shows schematically the position of the targets in the scenario proposed. Figs.8b-c shows the range-Doppler map in dB when the rotation corner is stopped (Fig.8b) or in movement (Fig.8c). Considering a value of D=0.05 m and a f_r=15 Hz (1000 rpm), a modulation index β =20 is obtained. The small RCS of the pedestrian is masked by trees, or other close objects, with higher RCS. However, the position of the pedestrian (or cyclist) can be identified by using a rotation corner. A nearly constant signature in the Doppler axis around the point in the range-Doppler without rotation extending a variation Δv=BW·c/(2f_c)=3.75 m/s is observed according to the theory presented. This particular Doppler signature is difficult to obtain with other targets, therefore it can be used to identify a rotation corner and warn the car of the close presence of a sensible target as road workers, pedestrians or cyclists.

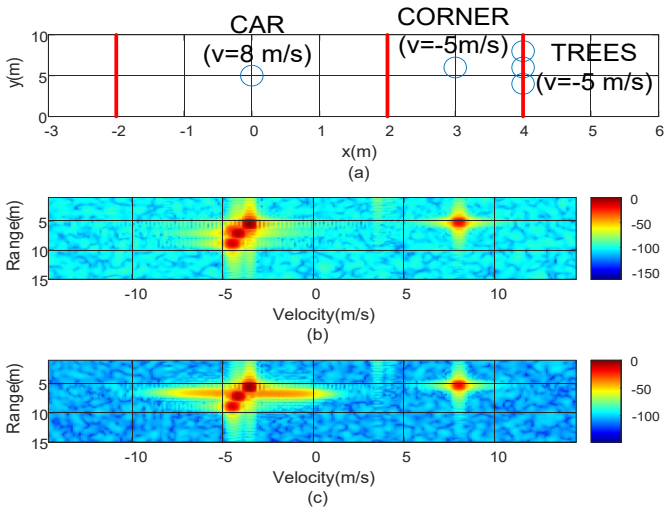

Fig. 8. (a) Locations and velocities of the targets, range-Doppler map in dB when the motor is Off (b) and On (case D=0.05 m, f_r=15 Hz)(c).

IV. Experimental results

Some experiments in the laboratory have been conducted in order to demonstrate the theory. A rotating circular trihedral prototype was made with a 3D printer and covered with conductive tape. These devices are characterized by their high RCS and nearly uniform angular behavior. The diameter of the corner is 15.75 cm and the theoretical maximum RCS is 6 dBsm at 24 GHz [10]. The device is connected to a DC motor (RS PRO Stock No: 321-3192). A Hall-effect sensor (Analog Devices AD22151) connected to an oscilloscope was used to characterize the rotation velocity of the transponder. The Hall sensor generates a voltage pulse every time that this is approached to a small magnet attached to the rotary table. Rotation frequency is obtained by measuring the pulse repetition frequency. The rotation velocity can be adjusted changing the voltage applied to the DC motor. An image of the rotating corner is shown in Fig.9. A FMCW radar at 24 GHz implemented in the EVAL-DEMORAD from Analog Devices was used for performing the measurements. The radar sweeps from 24-24.3 GHz with a sampling frequency of 1.2 MHz and a sweep time of 250 µs. The points per frame were 256 and a total of 128 frames were used.

Fig.10 shows the measured range-velocity maps performed in the laboratory using the radar located at 1.5 m from the corner, considering four rotation velocities: 0 rev/min, 460 rev/min, 955 rev/m, 1320 rev/m. Fig.11 shows a cut for the range 1.5 m as a function of the velocity for the four measurements. An increase of the bandwidth in velocity Δv proportional to the rotation frequency is observed. On the other hand, a discrete behavior can be observed too, especially at higher rotation frequencies, because the radar presents enough velocity resolution to distinguish the spectral lines. A comparison between the theoretical bandwidth considering D equal to the radius of the corner (15.75/2 cm) and measurements derived from the rotation velocities is shown in Fig.12. Despite the simplified theory presented, the spectrum bandwidth is in agreement with measurements.

TABLE I
Parameters used in the simulation of the scenario

Parameter	Value
Frequency Range (GHz)	24-24.3
Transmitter power (dBm)	8
Tx, Rx antenna Gain (dBi)	13.2
Azimuth beam width -3 dB (deg)	76.5
Sampling frequency (MHz)	1.2
Sweep time T (µs)	256
Number of samples per chrip N	256
Number of chiprs per frame L	128
Radar velocity (m/s)	5
Car RCS (dBsm)	18
Car velocity (m/s)	13
Corner RCS (dBsm)	6
Corner velocity (m/s)	0
Tree RCS (dBsm)	10
SNR (dB) for 0 dBsm target at 5 m	6

Fig. 9. Photography of the rotation corner used in the experiments.

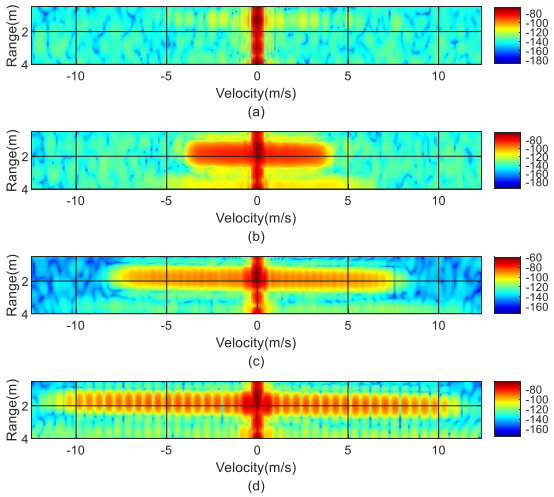

Fig. 10. Measured Range-Doppler map in dB with the motor off (a) and the motor on for different rotation velocities: (b) 460 rev/m, (c) 954 rev/min, (d) 1320 rev/min.

Measurements have been performed in three scenarios. The first scenario, shown in Fig.13, is a street where the rotating corner (tag) is located close to a guardrail. Fig.14 shows measurements in scenario 1. The experiment considers two motor states (at 0 and 1000 rev/m), with the rotating corner at 8 m from the radar. The large reflections due to clutter, guardrail, posts, and ground make difficult the identification of the tag when the motor is motionless. Fig.15 shows the measurement of the rotating corner with the motor on (at 1000 rev/min) located at 12 m from the radar in scenario 1.

Fig. 15b corresponds to a measurement with a pedestrian walking to the radar in front of the corner. This behavior allows distinguishing the rotating corner from other objects even if the RCS of these objects is higher than the transponder and therefore warns of the presence of a person associated with the rotating reflector, demonstrating the advantages of the proposed solution.

Fig.16 shows photography of the second scenario. In this case, the rotating corner is located at 8 m just in front of a parked car in the street that produces a strong reflection, but the backscatter on top of the cone continues being detected, as shown in Fig.17. This figure shows the measurements with the motor on without traffic (Fig.17a) but also with another car passing near the corner (Fig.17b) that introduces a cloud of reflections.

Fig.18 shows an experiment with the radar onboard a vehicle in movement. The measurement sets the rotating backscatter with the motor on (1000 rev/m) on top of a cone, close to the guardrail similar to scenario 1. Now, the response is observed shifted towards negative velocity, due to the radial velocity of the corner approaching the vehicle in movement. However, the characteristic signature in the Doppler domain allows to identify it, demonstrating that the identification enhancement continues to be effective in a non-static situation. We are using a low velocity for the sake of safety.

Fig.19 shows a typical scenario (scenario 3) with a car standing at the edge of the road close to a guardrail. The corner with the motor on is located in front of the car to highlight its position. The radar is mounted in a car that is moving toward the corner parallel to the guardrail. Fig. 20 shows measurement in this scenario where the corner is located at 15 m from the radar. In this case, a shift in the corner response due to the Doppler effect associated with the movement can be observed. The strong reflection of the guardrail makes difficult the identification of the standing car. However, the signature of the corner is clearly identified.

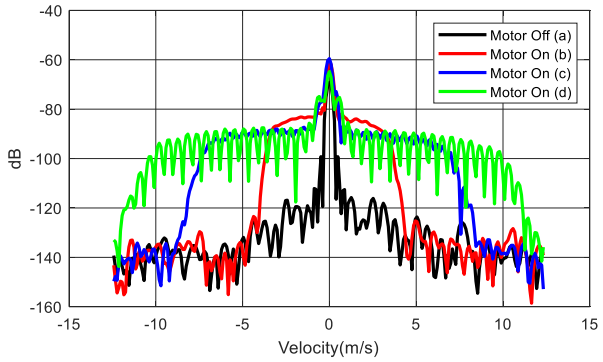

Fig. 11. Cut of the Range-Doppler of Fig.10 at range 1.5m comparing the response in the velocity axis with motor is Off and On.

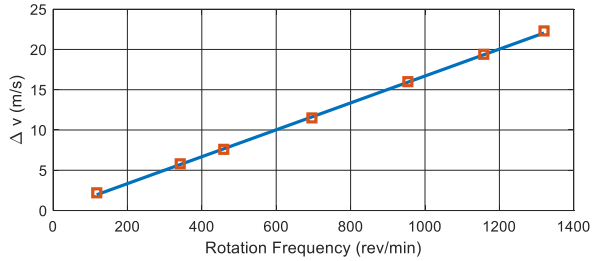

Fig. 12. Comparison of the measured velocity bandwidth (□) and theoretical expression from the measured rotation velocity.

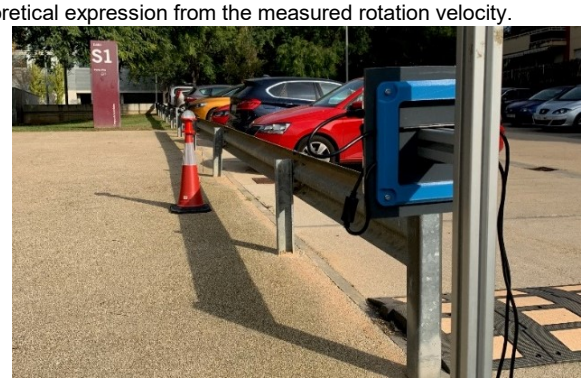

Fig. 13. Photography of the scenario 1 in a street with a guardrail with the rotating corner mounted on a safety cone.

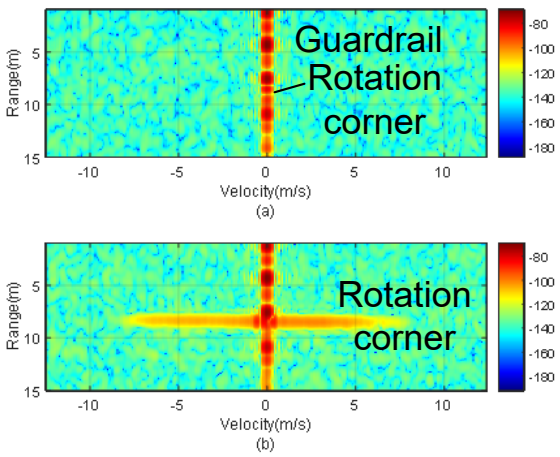

Fig. 14. Measured range-Doppler range map in scenario 1 where the tag is located at 9 m with the motor off (a) and with the motor on (b).

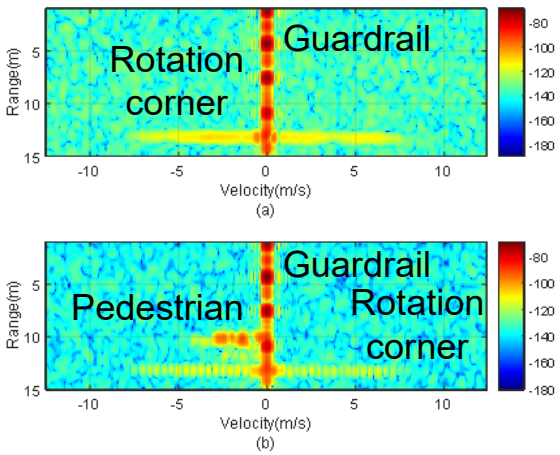

Fig. 15. Measured range-Doppler range map in scenario 1 where the tag is located at 12 m with the motor on (a) and with a pedestrian walking close to the tag (b).

Fig. 16. Photography of scenario 2 with the rotating corner mounted on a safety cone in front of a car.

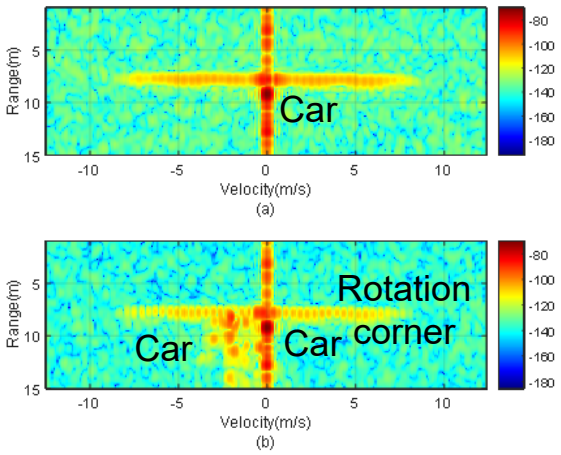

Fig. 17. Measured range-Doppler range map in scenario 2 where the tag is located at 8 m with the motor off (a), and with another car driving down the street in front of the tag (b).

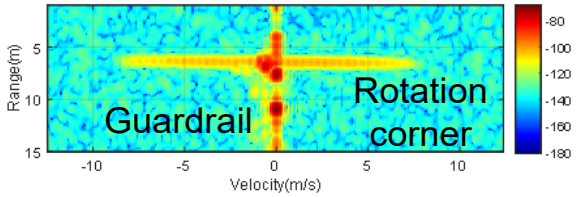

Fig. 18. Measured range-Doppler range map in scenario 1 where the tag is moving to the radar at 6 m of distance.

Fig. 19. Photography of scenario 3 with the rotating corner mounted on a safety cone near a guardrail and the radar mounted in a car.

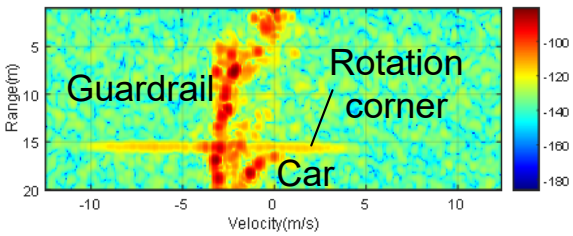

Fig. 20. Measured range-Doppler range map in scenario 3 where the tag is located close to a stopped car close to a guardrail. The radar is mounted in a car that is moving towards the tag parallel to the guardrail.

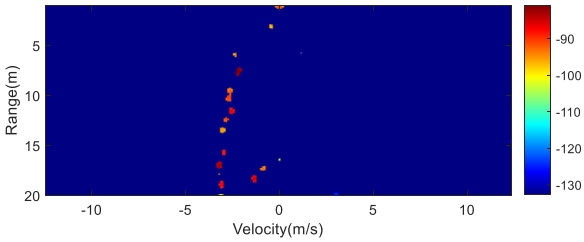

Fig. 21. Output of CFAR processor for the range-Doppler map of Fig.20.

From the range-Doppler map, automotive radars use constant false alarm rate (CFAR) techniques to detect the targets [23]. The aim of the CFAR algorithm is to determine the threshold above which the signal can be considered a target. Different CFAR processors have been proposed to perform this estimation. The well-known cell-averaging constant false alarm rate (CA-CFAR) noise estimation is based on averaging the values of the cells in the training area. CA-CFAR is applied in both dimensions (range and Doppler). The signal returned from the rotating corner spreads the energy in the Doppler direction. This will be considered like a noise, and hence it will be filtered when the averaging is performed. Fig. 21 shows the results after the CA-CFAR processor is applied to the range-Doppler map of Fig. 20. The threshold was set to 10 dB over the noise estimated from the output of a classic CA-CFAR algorithm. A total of 10 averaging and 5 guard cells in range and velocity have been used respectively. The target related to the structural mode that is RCS' average of the corner including its support is detected. Similar results have been obtained used standard CFAR processors such as the ordered statistic constant false alarm rate (OS-CFAR). Therefore, it can be concluded that the rotation corner does not interfere with the automotive radar, but a detection algorithm must be designed to detect it. The algorithm should have low computational cost and should be compatible with the standard automotive signal processing techniques that will allow the implementation in embedded platforms.

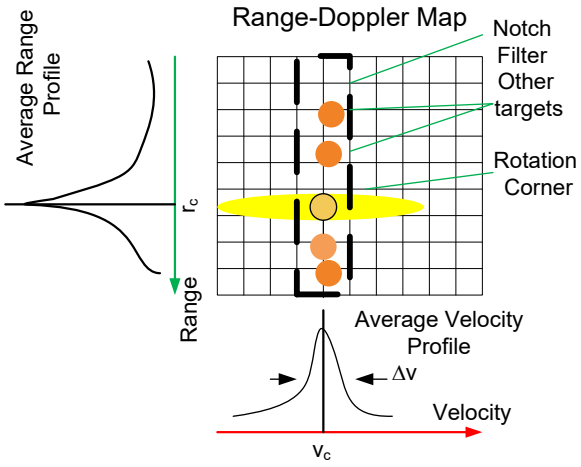

Fig. 22. Schema of rotating transponder detector based on a filter in Doppler and the average range profile.

Fig. 22 shows schematically the main steps of the detection algorithm. It is based on a notch filter in Doppler direction that removes the undesired targets. The strongest targets associated to moving cars can be removed using the CFAR algorithm. Therefore, a cleaned range-Doppler matrix (RD_{ik}) consisting of the cells that are below of the adaptive threshold obtained from the CFAR algorithm is used as the starting point of the detection algorithm. However, residual clutter is still present. These points are removed using an ideal notch filter. The center of the band is estimated from the centroid of the average velocity profile (AVP). This centroid will be close to the average relative velocity of the vehicle equipped with the radar. The AVP profile is obtained from the sum by columns of the cleaned range-Doppler map (see Fig. 22):

$$AVP(v_k) = \frac{1}{N}\sum_{i=1}^{N}|RD_{ik}|^2 \qquad (13)$$

Where N is the number of cells in velocity axis and RD_{ik} is the range-Doppler map at the cell with velocity v_k and range r_i. The bandwidth of the filter is adjusted automatically taking 20 times the standard deviation of the AVP. Then, the notch filter is applied. The average range profile is obtained by summing the rows of the filtered range-Doppler map (see Fig. 22).

$$ARP(r_i) = \frac{1}{M}\sum_{k=1}^{M}|RD_{ik}|^2 \cdot |H_{ik}|^2 \qquad (14)$$

Where M is the number of cells in range and H_{ik} is the transfer function of the notch filter. In absence of the rotating corner, the result shows a nearly constant value corresponding to the averaged clutter and noise. However, in presence of a rotating corner, a peak at the range position of the transponder (r_c) is obtained.

Fig. 23 compares the average range profile obtained for the range-Doppler shown in Fig. 14 considering or not the rotating transponder. Figs. 24-25 show the average range profile obtained for the range-Doppler shown in Figs. 19-20, respectively. These figures demonstrate that it is possible to detect the presence of the rotation corner from a simple threshold, whereas the position can be obtained from the maximum of ARP. Typically, signal to noise higher than 20 dB ratio is obtained for the measured cases. Note that the detection algorithm is compatible with standard techniques used in automotive radar and allows to automatically obtain the presence of the rotation corner and the distance at which it is located, without any training or complicated parameter selection.

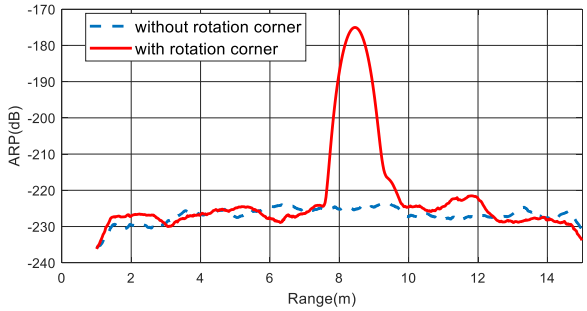

Fig. 23. Average range profile corresponding to the case of Fig. 14 with and without the presence of the rotation corner.

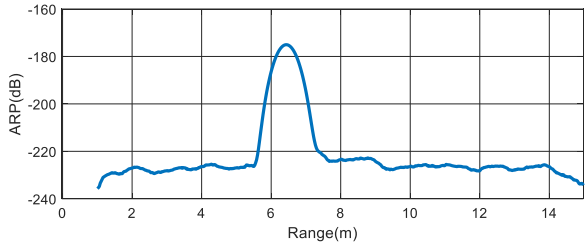

Fig. 24. Average range profile corresponding to the case of Fig. 19.

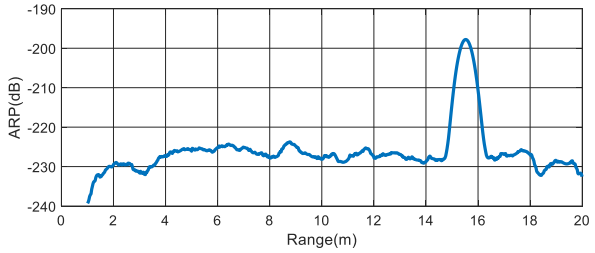

Fig. 25. Average range profile corresponding to the case of Fig. 20.

V. Conclusions

This paper proposes the use of rotating corners as a modulated transponder tag to improve the identification by automotive FMCW radar of objects with small RCS that can be masked by other objects. The theory of operation with FMCW radars has been presented and has been validated with simulations and experimental results at 24 GHz. A wideband spectrum in Doppler allows the identification of the transponder from other objects. The level of RCS can be adjusted with the dimensions of the corner and their fabrication is easy in comparison with other active transponders. As the RCS increases with the frequency, the corner can be used with a great range of frequency bands. Higher range detectability can be achieved at 77 GHz in long-range radar compared to short-range radars at 24 GHz due to the higher RCS of the corners. A simple detection algorithm has been proposed for the automatic detection of the presence of a rotation corner from the measured range-Doppler map. Increasing the size (diameter) of the

rotating corner and the rotation velocity, the bandwidth in Doppler increases. Therefore, the energy is spread in Doppler making its detection difficult with standard CFAR processors because the signal is confused with the background noise. Therefore, the interference in the radar is cancelled. However, the proposed technique based on the integration of the energy in Doppler allows to detect the rotating motor although the RCS of the corner is not very high. The main limitation of the proposed system is the power consumption associated with the motor. The batteries required to supply this motor and their lifetime can be a problem for some applications if there are not access to another power source. A low power consumption electronic version can be explored in future works based on other modulated backscatters. Therefore, the transponder could be held by pedestrians, cyclists, or as warning signals to indicate the presence of workers on the road. It can be used to enhance the detection in range-velocity maps used in automotive radars of pedestrians or other objects that can be masked by strong clutter.

REFERENCES

[1] W. J. Fleming, "New Automotive Sensors—A Review," *IEEE Sens. J.*, vol. 8, no. 11, pp. 1900–1921, Nov. 2008.

[2] EC–European Comission, "Towards a European road safety area: Policy orientations on road safety 2011-2020," *COM (2010), vol.389*, 2010.[Online]. Available: https://ec.europa.eu/transport/road_safety/sites/roadsafety/files/pdf/com_20072010_en.pdf. [Accessed: 08-Jan-2020].

[3] S. Heuel and H. Rohling, "Pedestrian classification in automotive radar systems," in *Proceedings International Radar Symposium*, 2012, pp. 39–44.

[4] Z. Slavik and K. V Mishra, "Phenomenological Modeling of Millimeter-Wave Automotive Radar," in *2019 URSI Asia-Pacific Radio Science Conference (AP-RASC)*, 2019, pp. 1–4.

[5] C. Beck *et al.*, "Industrial mmWave Radar Sensor in Embedded Wafer-Level BGA Packaging Technology," *IEEE Sens. J.*, vol. 16, no. 17, pp. 6566–6578, 2016.

[6] I. Matsunami, R. Nakamura, and A. Kajiwara, "RCS measurements for vehicles and pedestrian at 26 and 79GHz," in *2012 6th International Conference on Signal Processing and Communication Systems*, 2012, pp. 1–4.

[7] E. Marchetti *et al.*, "Comparison of pedestrian reflectivities at 24 and 300 GHz," in *Proceedings International Radar Symposium*, 2017.

[8] L. R. and T. Z. T. Schipper, J. Fortuny-Guasch, D. Tarchi, *Proceedings of the Fourth European Conference on Antennas and Propagation CCIB, Barcelona, Spain, 12-16 April 2010.* EurAAP, 2010.

[9] J. Lin, S. Chien, Y. Chen, C. Chen, and R. Sherony, "24 GHz and 77 GHz Radar Characteristics of Metal Guardrail for the Development of Metal Guardrail Surrogate for Road Departure Mitigation System Testing," in *2019 IEEE Intelligent Transportation Systems Conference (ITSC)*, 2019, pp. 3340–3346.

[10] U. Chipengo, "Full Physics Simulation Study of Guardrail Radar-Returns for 77 GHz Automotive Radar Systems," *IEEE Access*, vol. 6, pp. 70053–70060, 2018.

[11] C. Liu, S. Liu, C. Zhang, Y. Huang, and H. Wang, "Multipath Propagation Analysis and Ghost Target Removal for FMCW Automotive Radars," in *22020 IET Int. Radar Conf. (IRC), Chongqing, China, November 4–6, 2020*, 2020.

[12] V. C. Chen, "Analysis of radar micro-Doppler with time-frequency transform," in *Proceedings of the Tenth IEEE Workshop on Statistical Signal and Array Processing (Cat. No.00TH8496)*, 2000, pp. 463–466.

[13] M. R. Bell and R. A. Grubbs, "JEM modeling and measurement for radar target identification," *IEEE Trans. Aerosp. Electron. Syst.*, vol. 29, no. 1, pp. 73–87, 1993.

[14] T. Shan, S. Liu, R. Tao, and G. Zhang, "Experiment demonstration of micro-Doppler detection of rotor blades with passive coherent location based on digital video broadcast," *J. Commun. Technol. Electron.*, vol. 59, no. 11, pp. 1215–1224, 2014.

[15] D. Belgiovane and C. Chen, "Micro-Doppler characteristics of pedestrians and bicycles for automotive radar sensors at 77 GHz," in *2017 11th European Conference on Antennas and Propagation (EUCAP)*, 2017, pp. 2912–2916.

[16] S. Park *et al.*, "Combination of radar and audio sensors for identification of rotor-type Unmanned Aerial Vehicles (UAVs)," in *2015 IEEE SENSORS*, 2015, pp. 1–4.

[17] F. Hoffmann, M. Ritchie, F. Fioranelli, A. Charlish, and H. Griffiths, "Micro-Doppler based detection and tracking of UAVs with multistatic radar," in *2016 IEEE Radar Conference (RadarConf)*, 2016, pp. 1–6.

[18] Z. Tao and Q. Fu, "Discrimination Method of Ship and Corner Reflector Based on Micro-Doppler Feature," in *Proceedings of the 2016 International Conference on Computer Engineering, Information Science & Application Technology (ICCIA 2016)*, pp. 508–513.

[19] E. F. Knott, *Radar Cross Section Measurements*. Springer US, 1993.

[20] J. N. Briggs, *Target detection by marine radar*, vol. 16. Iet, 2004.

[21] E. Hyun, Y.-S. Jin, and J.-H. Lee, "A Pedestrian Detection Scheme Using a Coherent Phase Difference Method Based on 2D Range-Doppler FMCW Radar," *Sensors*, vol. 16, no. 1, p. 124, Jan. 2016.

[22] M. Kronauge and H. Rohling, "Fast Two-Dimensional CFAR Procedure," *IEEE Trans. Aerosp. Electron. Syst.*, vol. 49, no. 3, pp. 1817–1823, 2013.

[23] S. Li, X. Bi, L. Huang, and B. Tan, "2-D CFAR Procedure of Multiple Target Detection for Automotive Radar." 2017.

Antonio Lazaro (M'07–SM'16) was born in Lleida, Spain, in 1971. He received the M.S. and Ph.D. degrees in telecommunication engineering from the Universitat Politècnica de Catalunya (UPC), Barcelona, Spain, in 1994 and 1998, respectively. He then joined the faculty of UPC, where he currently teaches a course on microwave circuits and antennas. Since July 2004, he is a Full-Time Professor at the Department of Electronic Engineering, Universitat Rovira i Virgili (URV), Tarragona, Spain. His research interests are microwave device modeling, on-wafer noise measurements, monolithic microwave integrated circuits (MMICs), low phase noise oscillators, MEMS, RFID, UWB and microwave systems

Marc Lazaro was born in Tarragona, Spain, in 1995. He received the BS in Industrial Electronics and Automation Engineering and the MS in Electronic Systems Engineering and Technology (METSE) from Rovira i Virgili University, Tarragona, Spain, in 2017 and 2018, respectively. Up until now, he has accumulated professional experience as a data acquisition engineer and as embedded systems developer. Since 2019 he has been working toward the Ph.D. degree in the Department of Electronics at the Rovira i Virgili University. His research activities are focused on semipassive RFID technologies based on backscattering communication and novel applications based on Millimeter-wave identification (MMID).

Ramon Villarino was awarded a degree in Telecommunications Technical Engineering by Ramon Llull University (URL) in Barcelona, Spain, in 1994, a degree in Senior Telecommunications Engineering by the Universitat Politècnica de Catalunya (UPC) in Barcelona, Spain, in 2000 and a doctorate by the UPC in 2004. In 2005-2006, he was a Research Associate at the Technological Telecommunications Center of Catalonia (CTTC) in Barcelona, Spain. He worked as a Researcher and Assistant Professor at the Universitat Autònoma de Barcelona (UAB) from 2006 to 2008. Since January 2009 he has been a full-time professor at Universitat Rovira i Virgili (URV) in Tarragona, Spain. His

research activities focus on radiometry, microwave devices, and systems based on UWB, RFIDs, and frequency selective structures using MetaMaterials (MM).

Pedro de Paco (M'18-SM20) was born in Badalona, Spain. He received M.S. degree in Telecommunication Engineering in 1997 and a Ph.D. degree (Cum Laude) in 2003 from the Universitat Politècnica de Catalunya (UPC).

In 1998, he joined the Electromagnetic and Photonics Engineering Group (EEF), signal theory and communications department (TSC-UPC) with a grant from the Institut d'Estudis Espacials de Catalunya (IEEC) in a joint activity related with the European scientific space mission Planck. He was member of the LFI-Radiometer working group and the Planck Consortium. During his PhD and UPC stage participated in several national and international research projects mostly related to microwave and millimeter-wave circuits and systems applied to design and testing of remote sensing instruments and front-end point-to-multipoint broad-band communication system.

From 2004 he has been Associate Professor at the Universitat Autònoma de Barcelona where he teaches applied electromagnetics and microwave engineering courses. Awarded 3 times with merits in research and recognized with merits in University training by l'Agència de Qualitat, and awarded with Advanced Research by Generalitat Catalunya. He has advised 8 PhD students. From 2010-2013 he was deputy director and member of the Executive Board in the Telecommunication and System Engineering Department at UAB. During 2018-2019 he was a Visiting Researcher with the Microwave and RF Research Group, Colorado University-Boulder (US). He has been appointed as technical expert for Telecommunications Equipment by National Agency of Accreditation. He is member of MTT-6 RF MEMS and Microwave Acoustics Committee, reviewer for IEEE Transactions on Microwave Theory and Techniques, IEEE Microwave and Wireless Components Letters. He serves as a member of the Technical Review Board for the European Microwave Conference. His main research interests include Microwave filter synthesis and Microwave Acoustics filter synthesis and design, as well as Microwave and Radar systems and devices.